SAND2020-8326R

Sandia National Laboratories

National Nuclear Security Administration

# Research Performance Progress Report (RPPR-1)

| | | |
|---|---|---|
| **a. Federal Agency** | Department of Energy | |
| **b. Award Number** | 34367 | |
| **c. Project Title** | Optimized Bifacial PV Systems | |
| **d. Principal Investigator** | Joshua S. Stein<br>Lead PI<br>jsstein@sandia.gov<br>(505) 379-0895 (cell) | |
| **e. Business Contact** | Brion Bob | |
| **f. Submission Date** | July 15, 2020 | |
| **g. DUNS Number** | 080645806 | |
| **h. Recipient Organization** | Sandia National Laboratories and National Renewable Energy Laboratory | |
| **i. Project Period** | **Start:** 10/1/2018 | **End:** 9/30/2021 |
| **j. Reporting Period** | **Start:** 1/1/2020 | **End:** 6/30/2020 |
| **k. Report Term or Frequency** | biannual (twice a year) | |
| **l. Submitting Official Signature** | | |

## Major Goals & Objectives:

This project has four main technical objectives:

- Develop and improve bifacial performance models by adding the capability to evaluate electrical behavior and performance of bifacial modules and arrays under realistic field conditions including irradiance variability caused by racking, module frame, and position in the array.
- Instrument and monitor performance of fielded bifacial systems to validate performance models and to measure, analyze and publish on bifacial energy gain. These should include both research and commercial bifacial systems and cover a variety of deployment applications.
- Evaluate optimal bifacial system designs using simulations leveraging high-performance computing, and also using full sized and miniaturized experimental field deployments.
- Establish and contribute to international test standards for bifacial system performance, testing, and safety, and work with the community to establish installation and siting best practices.

## Project Results and Discussion:

### Task 1. Bifacial Model Development and Analyses

*Bifacial_Radiance Updates*

The bifacial_radiance software has seen one new software release in Q2 and a second in Q3, improving spectral modeling capability and hourly ground-albedo importing capability. Software usage and downloads are increasing as internal and external publications and webinars feature the software. We are currently up to roughly 1500 page views and 75 new users per month (Figure 1).


*Figure 1 - Github statistics on downloads and views showing 145 unique visitors in the past 2-week period. Software downloads (github + pypi) : 75 / month*

Some of the latest functionalities added are modules with glass, for better consideration of Fresnel losses (captured in bifacialvf and other software packages through the Incident Angle Modifier) (Figure 2). Spectral simulation capability has also been added, as further explained in the next section. Agriphotovoltaics functionality tutorial was also added in April 2020 (Figure 3), with more dual-use modeling programmed for the future.

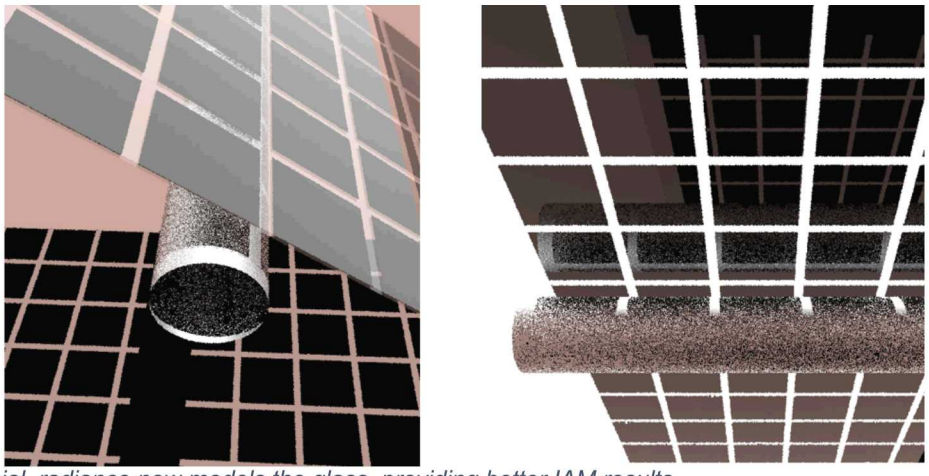

*Figure 2 - bifacial_radiance now models the glass, providing better IAM results.*

*Figure 3 - dual use of bifacialPV and agriculture is now included in bifacial_radiance tutorials.*

## *Spectral Modeling*

One of the main updates to bifacial_radiance is the ability to model the full spectrum of irradiance incident on the front and rear sides of modules (Figure 4). This feature is being used to analyze the impacts of albedo, scene object spectral reflectivity and spectral DNI + DHI on system performance. Input irradiance is spectrally resolved for DNI and DHI, using SMARTS2 and scaling the ideal DNI and DHI obtained for mostly sunny days, and SPCTRL2 for cloudy conditions. Spectrally resolved reflectivity (albedo) of different ground materials is also obtained from SMARTS2, and a correction factor is applied to the correct condition (i.e. brown grass) to match the field-measured albedo measured.

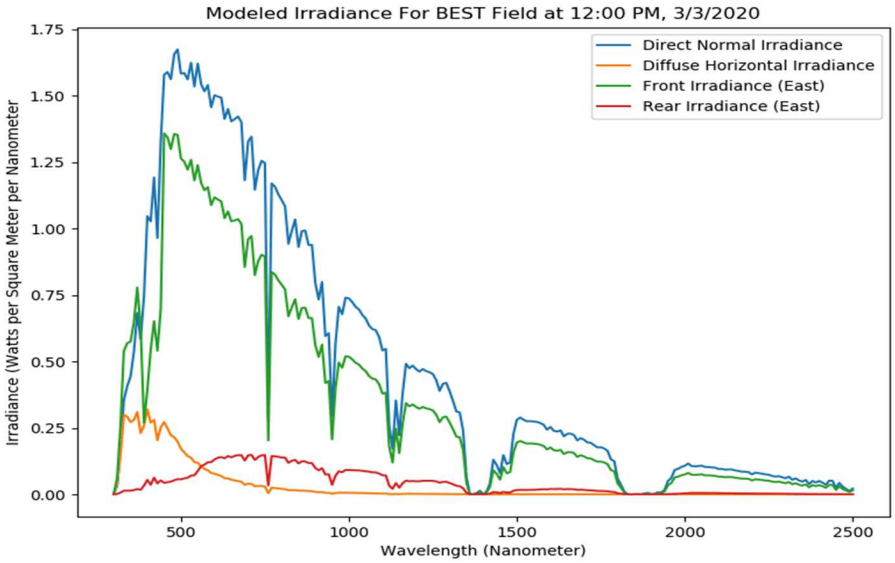


*Figure 4 - DNI and DHI spectra from SMARTS2 in blue and yellow. Front and rear spectrally resolved irradiance were simulated with bifacial_radiance for the 75kW field at NREL.*

Field results from the 75kW field at NREL show the importance of the location and spectral responsivity of the sensors used. Measurements show 8-13% irradiance variability in the rear-facing IMT-reference cell sensors (Figure 5**Error! Reference source not found.**). The broadband sensors show an increased 20% response relative to the reference cells. We are using bifacial_radiance to simulate this day considering the spectral response of the sensors and the spectrally resolved DNI, DHI, and albedo. Figure 6 shows the model results along with measurements for an example day. The model's underprediction for early and late hours is being investigated. NREL is also currently researching simpler methods of approximating the incident rear spectra and validating it with raytracing and field measurements.

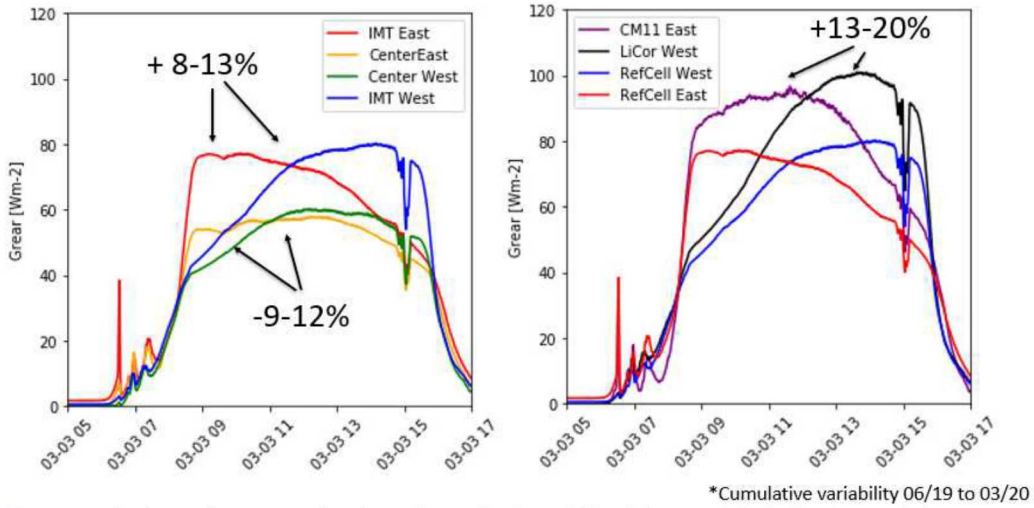


*Figure 5 - Four rear-facing reference cells along the collector width of the module indicate much lower rear irradiance (Grear) values in the center of the module than at the edges.*

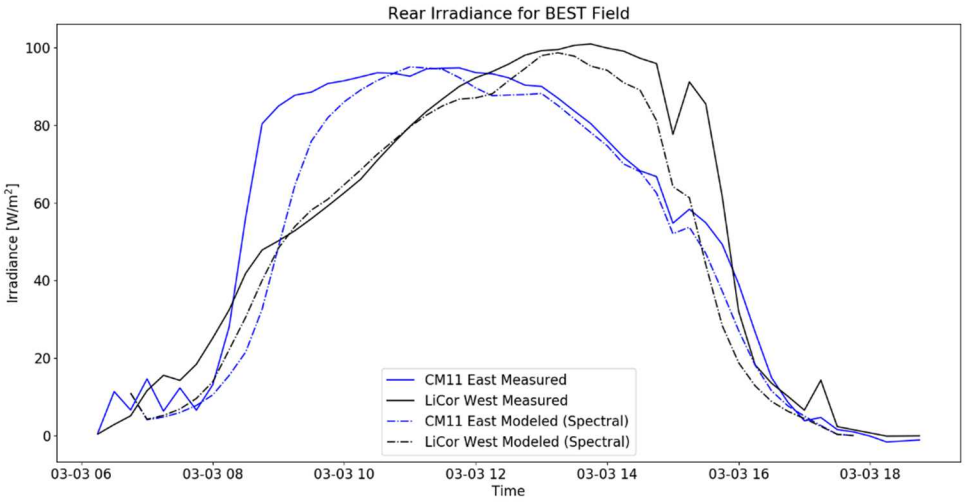


*Figure 6 - Measured rear-irradiance with two broadband irradiance sensors, located at the east- and west-most edges of the same module in the bifacial field at NREL. Spectrally resolved simulations show underprediction of the irradiance during the early and late hours of the day.*

## IEA PVPS Model Comparison

Sandia and NREL organized a model comparison exercise as part of the IEA PVPS Task 13 bifacial activity group. This exercise aimed at documenting current practice for modelling the performance of fielded bifacial photovoltaic systems. We invited participants from international research laboratories, universities, and industry to test their bifacial PV performance models on a common set of bifacial system designs, some of which have been deployed and monitored and some that are theoretical but represent a wide range of potential designs. Four main modeling scenarios were defined: south-facing fixed-tilt (S1), west-facing fixed-tilt (S2), east-west-facing vertical (S3), and horizontal single axis tracking (S4). In addition, there was an optional simulation based on real field data measured at NREL's bifacial single axis tracker field. Three locations with varying climate were also chosen, two are high DNI locations (one in north and one in south hemispheres), and the third one is a location at high latitude.

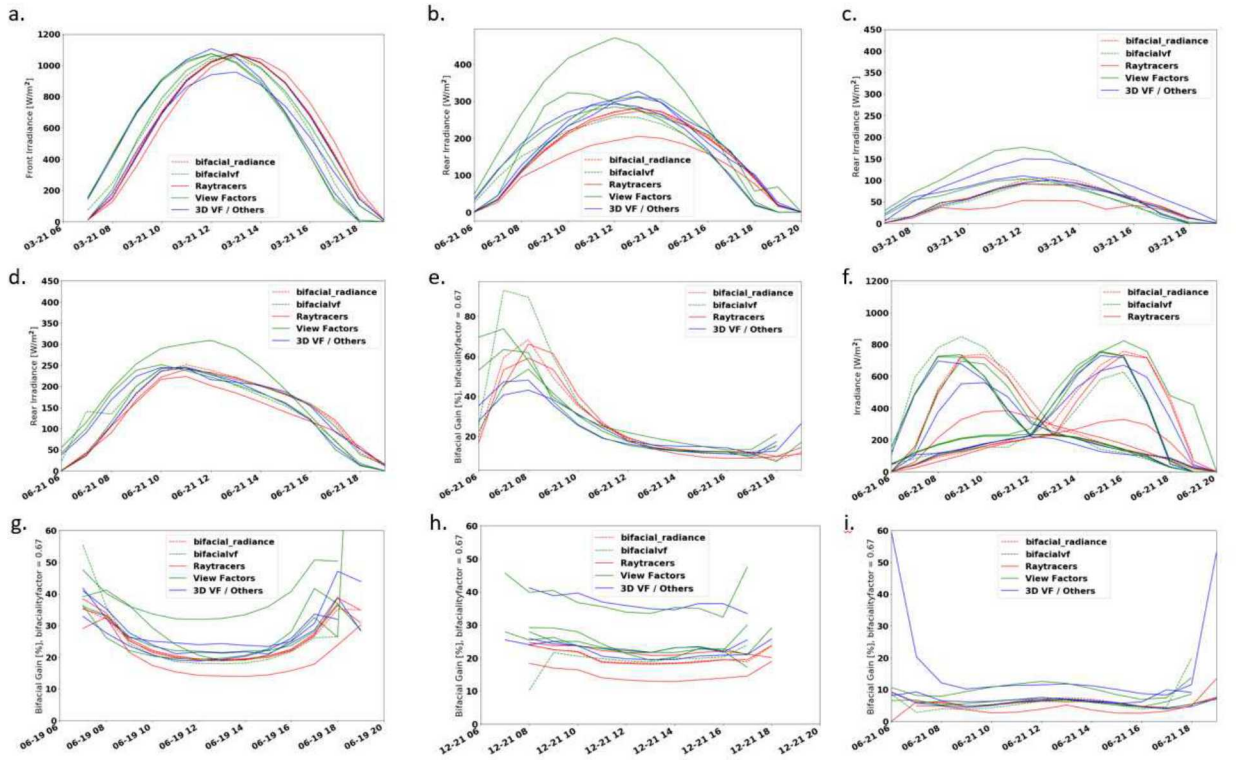


*Figure 7 - a) Front irradiance and b) rear irradiance for fixed-tilt system (spring equinox & summer solstice). c) Rear irradiance for tracking simulation, spring equinox. d) Front irradiance and e) rear irradiance for West-facing modules during summer Solstice. f) Vertical system at summer solstice. g) Bifacial Gain for fixed tilt system, for summer solstice and h) winter solstice. i) Bifacial gain for single axis tracked system.*

Selected representative results for S1-S4 are shown in Figure 7 for up to thirteen different bifacial modeling tools that were run. Rear irradiance results are shown in Figure 7(b), (c) and (e). Agreement between simulations seems to vary by 50 W/m$^2$ for early and late hours for rear irradiance, and 180 W/m$^2$ for front irradiance in S1, but this is mostly due to each software's selection of the exact timestamp to perform the modeling and select the sun positions. The hourly weather data used for these simulations represents hourly average irradiance reported at the end of each hour. Some models calculate sun positions 30 minutes prior to the reported timestamp, but this approach must be modified for the first and last hour of daylight.

The 75kW bifacial system at NREL was one of the optional modeling scenarios with real data for validation. Two raytracing models and four view factor models contributed results for this scenario, including bifacial_radiance, bifacialvf and SAM. Figure 8(*a)* shows the Global Horizontal Irradiance data used as input to the models. GHI was also used for aligning the results of the tools. Two sunny days and four days with intermittent clouds were modeled, with overall good agreement for front irradiance (Figure 8(*b)*). In Figure 8(*c)* and (*d)* we see the close-up of front irradiance for a sunny and cloudy day respectively. Three of the tools were limited to only modeling at hourly timesteps, which ignores the short-term variability in the 15-minute field data provided. Agreement between these models for front irradiance is between 30 W/m$^2$ for the front irradiance on the clear days.

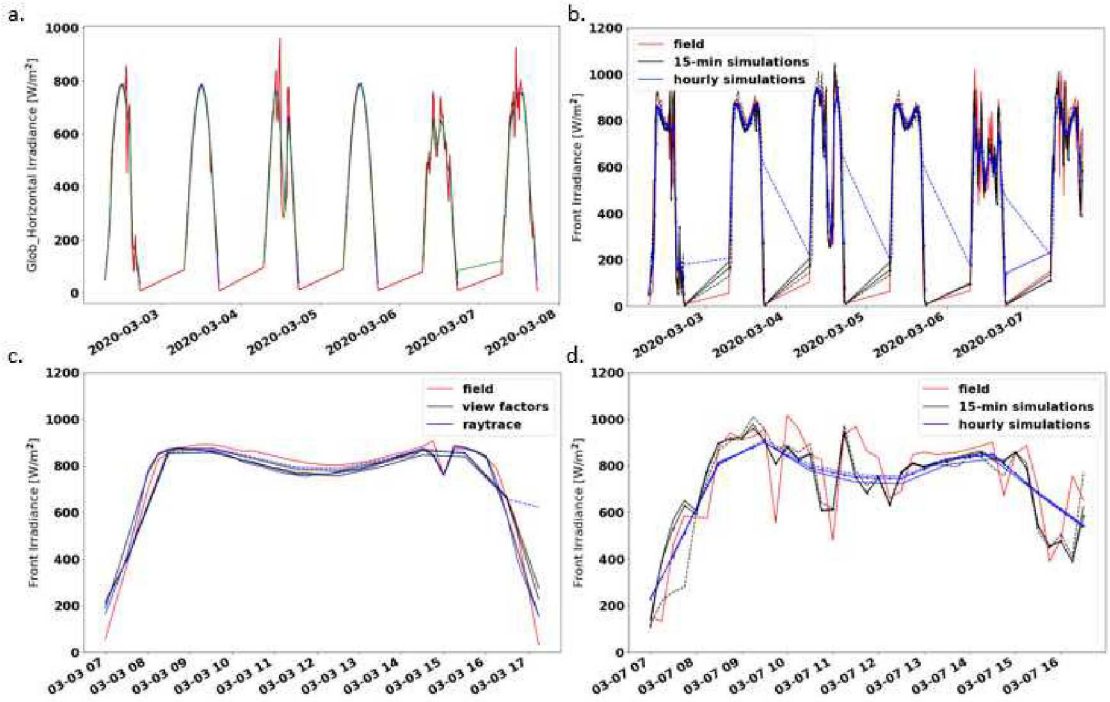


*Figure 8 - Results for optional simulation 2, including four view factor and 2 raytracing modeling tools. a) Global Horizontal data was used to properly align the results of all the tools. b) Front irradiance results.*

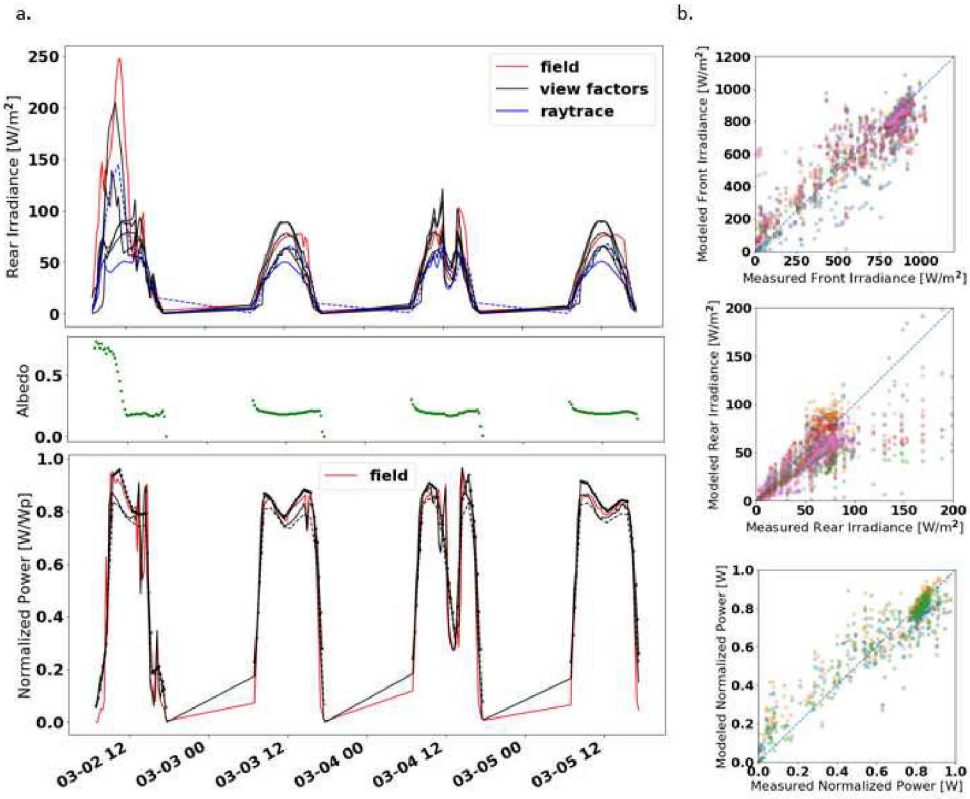


*Figure 9 - Optional simulation 3 results for a) rear irradiance and normalized power over four days, with albedo shown in green. b) modeled versus measured front rear irradiance and normalized power.*

Figure 9(*a)* shows rear irradiance results for the various models for Optional Simulation 2. Albedo on the first half of the first day is very high, causing the most severe underprediction of rear irradiance for the models. Normalized power production is also shown. Figure 9(*b)* shows measured vs. modeled results for front and rear. Rear results show a much higher deviation from measured for rear irradiances above 120 W/m$^2$, which are all measured on March 2nd before 1 PM.

## Task 2: Field Validation and Instrumentation of Bifacial Systems

### *Bifacial Experimental Single-Axis Tracking field results*

The 75kW bifacial field at NREL has now one year of data collected. Ten-month results were presented at the 47$^{th}$ PVSC, virtually on June as a live highlight session. As part of the results, the updated monthly results of the average of the PERC strings and silicon Heterojunction strings were shared. There is 7-9% cumulative bifacial energy gain for the 2 module types from July 2019 to April 2020. Figure 10 shows how SHJ outperforms the PERC technologies in summer due to the high temperatures and SHJ advantageous temperature coefficient. The bifacial gain disparity is lessened when the temperature drops starting in October. Both systems show increases in bifacial gain due to the increased albedo from snow starting in October. In particular, February recorded snow for most of the month, and that resulted in bifacial gains >15%.

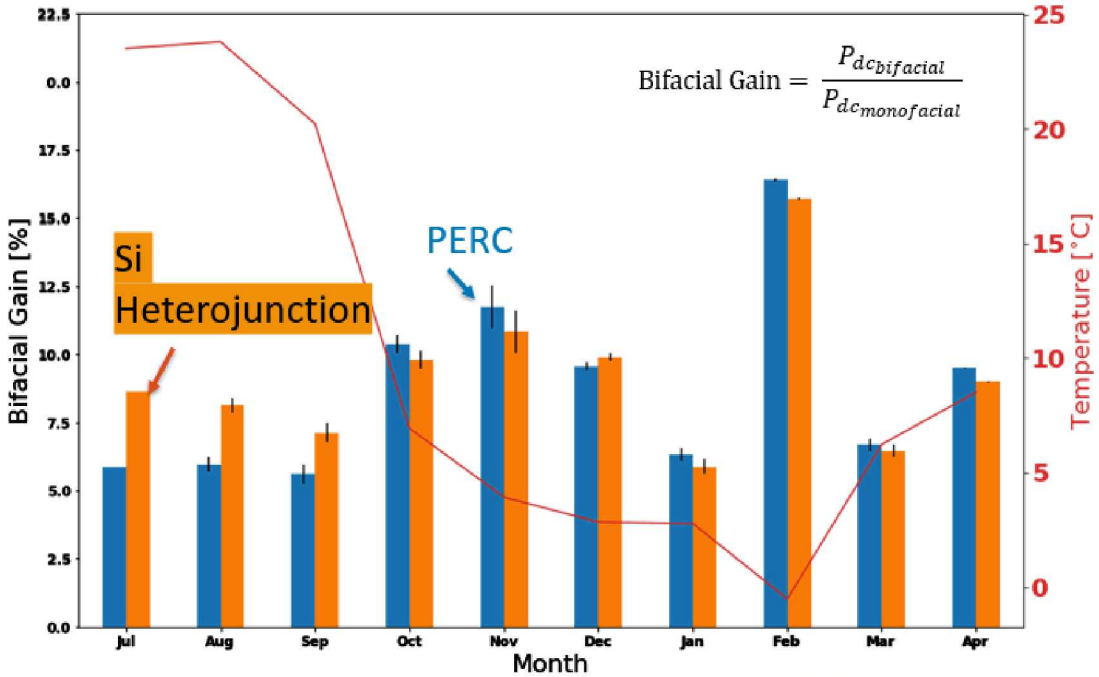


*Figure 10 - Bifacial gain comparison by technology. Cumulative bifacial gain: 7% (PERC) and 9% (SHJ)*

The module-level monitoring allowed us to look at the field performance with more detail under these snowy conditions. For the two days shown in Figure 11, the first day snow is falling, with low GHI values throughout the day. Despite the cloudiness from the snowfall, the bifacial modules

are producing power while the monofacial are not receiving enough light. The next day snow has covered the arrays. There is some ground reflected irradiance available early in the day, which allows the bifacial modules to produce power and shed snow earlier than the monofacial arrays.

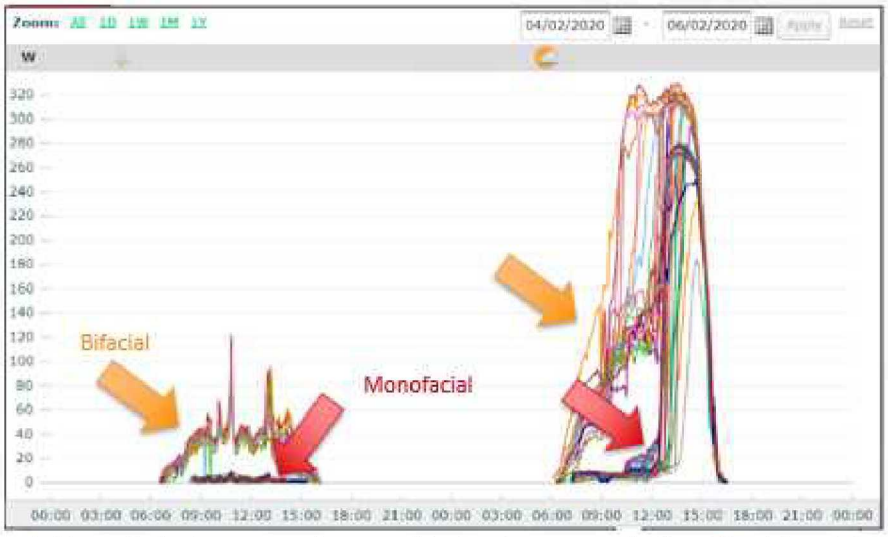


*Figure 11 - Tracker field results for two snowy days, module-level power production. Bifacial modules shed snow faster and produce more energy even when fully covered in snow.*

## Subtask 2.2: Evaluate field performance of sub-module-scale MPPT, module-scale MPPT, and string-scale MPPT for bifacial arrays

With the 75kw bifacial field data, we looked at the field-normalized production by aggregating the module-level data from January to May of this year, and then normalized all the rows by the average field production. By doing this we can immediately notice in Figure 12 which ones are the monofacial rows we are using for comparison in our array – rows 3, 6 and 8. And although there's a lot of variability caused by the module electronic monitors themselves, the edge effects are noticeable in the rows.

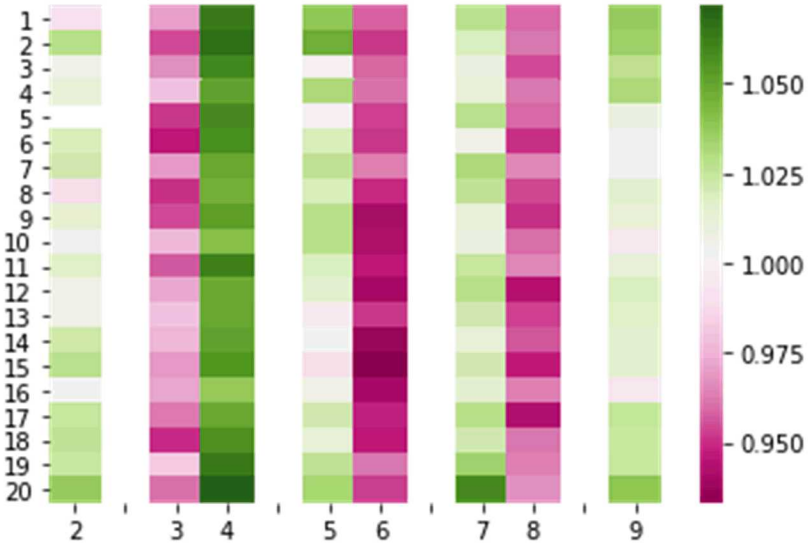


*Figure 12 - Field normalized production.*

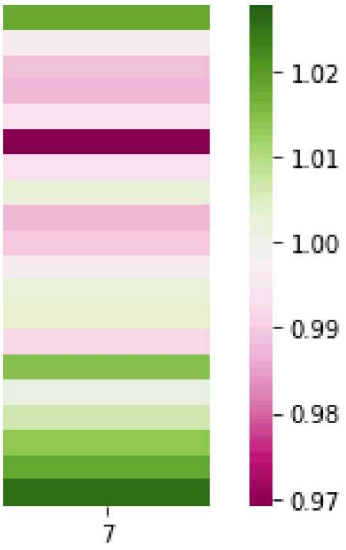


*Figure 13 - Edge effects shown on the south end of row 7 of the bifacial field for January-May module-level production data.*

In this closeup of row 7, each rectangle represents one of the modules, with the bottom of the heatmap being the south edge of the row, which receives more reflected light from the sun. The north module is also seeing increased irradiance. The increased irradiance translates to a 3% cumulative energy gain estimated for module-level power optimizers.

## *Public data on DuraMAT Datahub*

One year of data for two of the bifacial rows, as well as one of the monofacial rows for comparison is now publicly available in the DuraMat datahub (Figure 14). The data is accompanied by a user manual, which includes the site description and initial STC module measurements. One week of this data was leveraged for the IEC PVPS Task 13 bifacial model validation effort, further described in Task 1. Row level production data, front and rear irradiances and temperatures through the field, albedometers data, weather data from the Solar Radiation Research Laboratory

(located less than 100 meters from the field), as well as module-level production data for the two bifacial rows has been included.

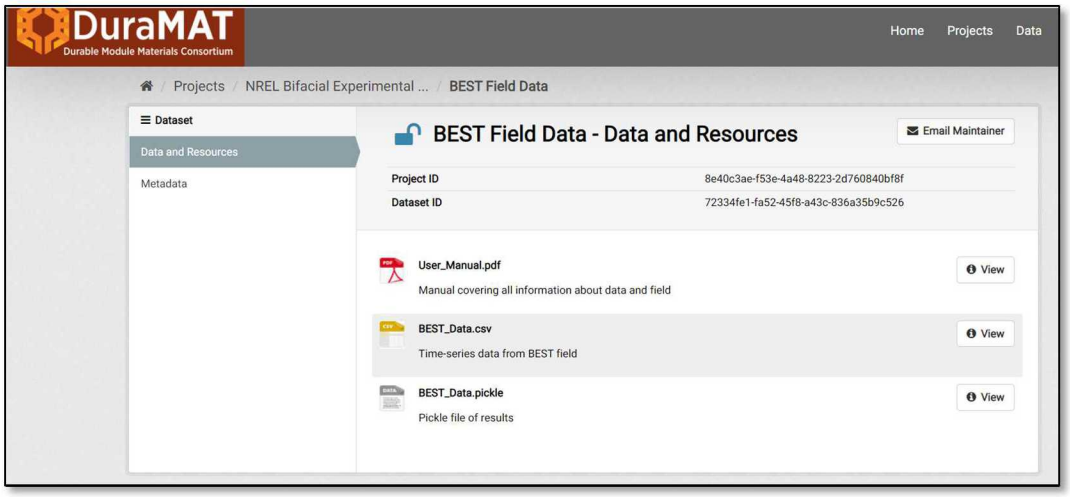


*Figure 14 - Data for the 75kW Bifacial Experimental Single-Axis Tracked field has been made available on DuraMAT Datahub (https://datahub.duramat.org/dataset/best-field-data)*

## Task 3. Computer Aided Design Optimization Studies for Bifacial Systems

### Subtask 3.1: Transfer models to the HPC environment and set up scripts to link to optimization engine

This task was largely completed in previous reporting periods. Both Sandia and NREL have bifacial_radiance running on their HPC clusters. Sandia has integrated the code into DAKOTA, which has the capability to run optimizations.

NREL participated in the Science Undergraduate Laboratory Internship Program this summer, with intern Mark Monarch who developed code to facilitate doing multiple simulations distributed in an independent fashion among all available cores, be it in a multi-core laptop or in the high-performance computing environment. His work on this multiprocessing package enabled results in Task 1 on spectral-raytrace with bifacial_radiance. This capability is seamlessly integrated in the current bifacial_radiance release and is also being tested for Amazon Web Services with full implementation and a training foreseen for next quarter.

### Subtask 3.2: Run optimizations for fixed tilt, ground mount; single axis and dual axis tracking

Prior to running a full optimization including cost implications of different designs. Sandia has been running a series of sensitivity studies to better understand how bifacial PV performance is affected by different design variables for fixed tilt, multi-row systems.

The initial set of simulations focused on the center module of a single south-facing row. The row initially consisted of only a single module with its rear irradiance simulated. A module was then added on either side of the center module for subsequent simulations of up to nine modules on either side of the central module. Albedo, tilt, and module height were held constant for this study

at 0.25, 35°, and 1 meter, respectively. The results in the show that the single isolated module is exposed to more than 45% more rear irradiation than the central module of a full row.

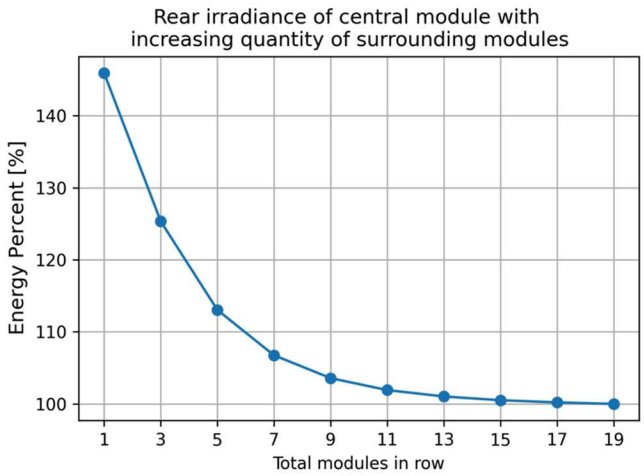


*Figure 15: The reduction in rear-side irradiation of center module caused by adding modules to a single row*

The next scenario studied was a south-facing row of 49 modules with irradiation simulated on the front and back of each module from the center module to the western-most module at the end of the row. We sequentially added identical rows of modules to the north and south of the first row and observed the effect on rear irradiation on modules in the center row. The ground albedo in this example is 0.25, height is 1 m, and tilt is 35°.
Figure 16 shows two important features of fixed-tilt, multi-row bifacial systems:

- Decrease in rear irradiation as rows increase: The rear-side irradiation at the middle of the row drops by over 15% as additional rows are added. The effect is most significant between the single row and three row case. However, adding more rows continues to slightly reduce rear irradiation.
- Increase in rear irradiation in modules near row edges: In the single-row example, the module nearest the edge experiences ~25% more rear-side irradiance than do the modules in the center of the row. Interestingly, the relative increase for edge modules is higher for the multi-row examples.

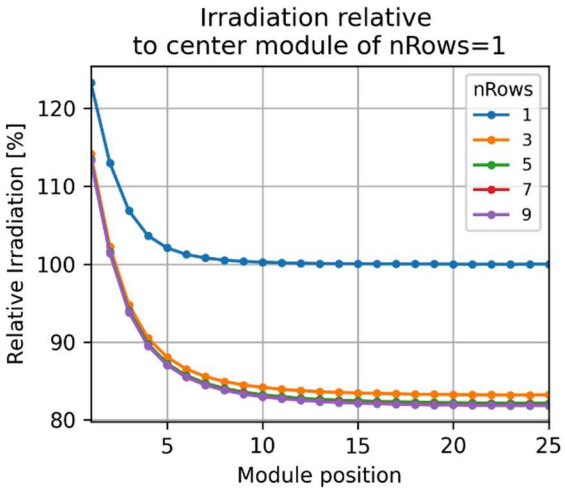


*Figure 16: Percent in rear-side irradiation relative to the center-most module of a single row system for systems with differing number of rows.*

## Role of albedo in multi-row fixed-tilt systems

The next set of simulations examined the role of albedo on rear-side irradiation in multi-row, fixed-tilt systems. This scenario simulated a single row at a 35° tilt angle at three different albedo values: 0.1, 0.25 and 0.8. Figure 17 compares the run results.

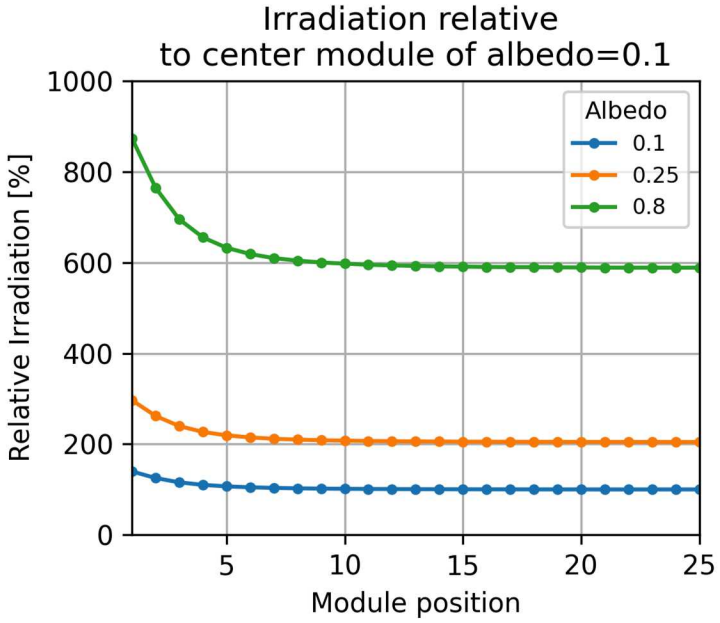


*Figure 17: Percent in rear-side irradiation relative to the center-most module in the array with an albedo of 0.1.*

Once again, there are two main conclusions from these runs. First, rear-side irradiance is highly correlated with albedo. Note that the relative increase in rear-side irradiance is slightly lower that

the relative increase in albedo. This reduction is due to the self-shading around the array. Second, the magnitude of the edge effect increases with albedo. This makes sense because modules on the edge are receiving more light from unshaded ground.

Next we looked at the relationship of tilt angle and rear-side irradiance by simulating five rows at 0.25 albedo with different tilt angles and correlated pitch value. It is commonly known that front-side insolation is typically maximized when the array tilt is close to the latitude of the site. For the rear-side, increasing tilt angle increases the proportion of the rear irradiance coming from the sky dome. In this example, back-side irradiance increased with tilt angle because the light coming from ground reflection is lower than the diffuse light coming from the sky. In the case of higher ground albedos, this pattern will change and may reverse when ground albedo is very high (e.g., with snow). Simulation results are shown in Figure 18.

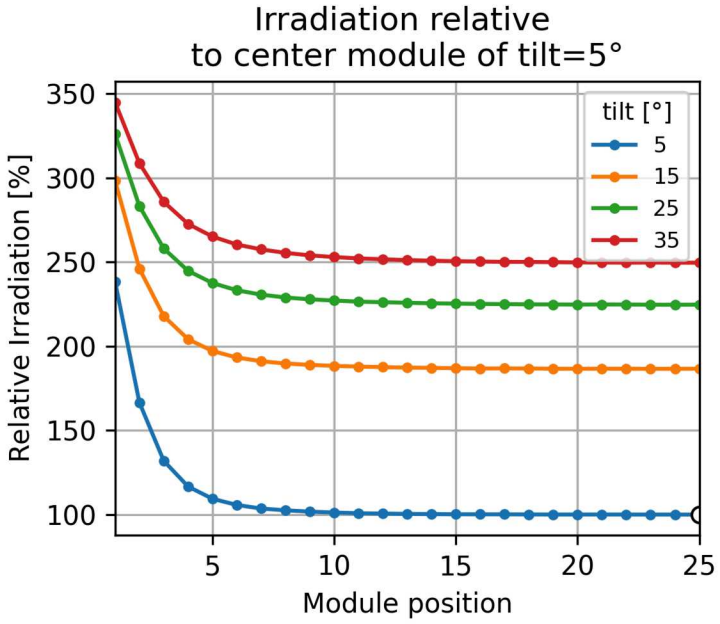


*Figure 18: Percent in rear-side irradiation relative to the center-most module in the array with a tilt angle of 5°.*

Next we ran a parametric study to show these effects across the array, not just the center row. Figure 19 shows a matrix of the western half of simulated arrays. Since the arrays are facing south, the eastern half is symmetrical to the western half. The numbers and their correlating color describe the relative percent increase in rear-side irradiance compared to the central module, considered a baseline reference as it receives the lowest rear irradiance. Each array within this matrix differs in tilt/pitch and height from the ground. Albedo is held constant at 0.8 for all arrays in this visualization but can be varied as necessary.

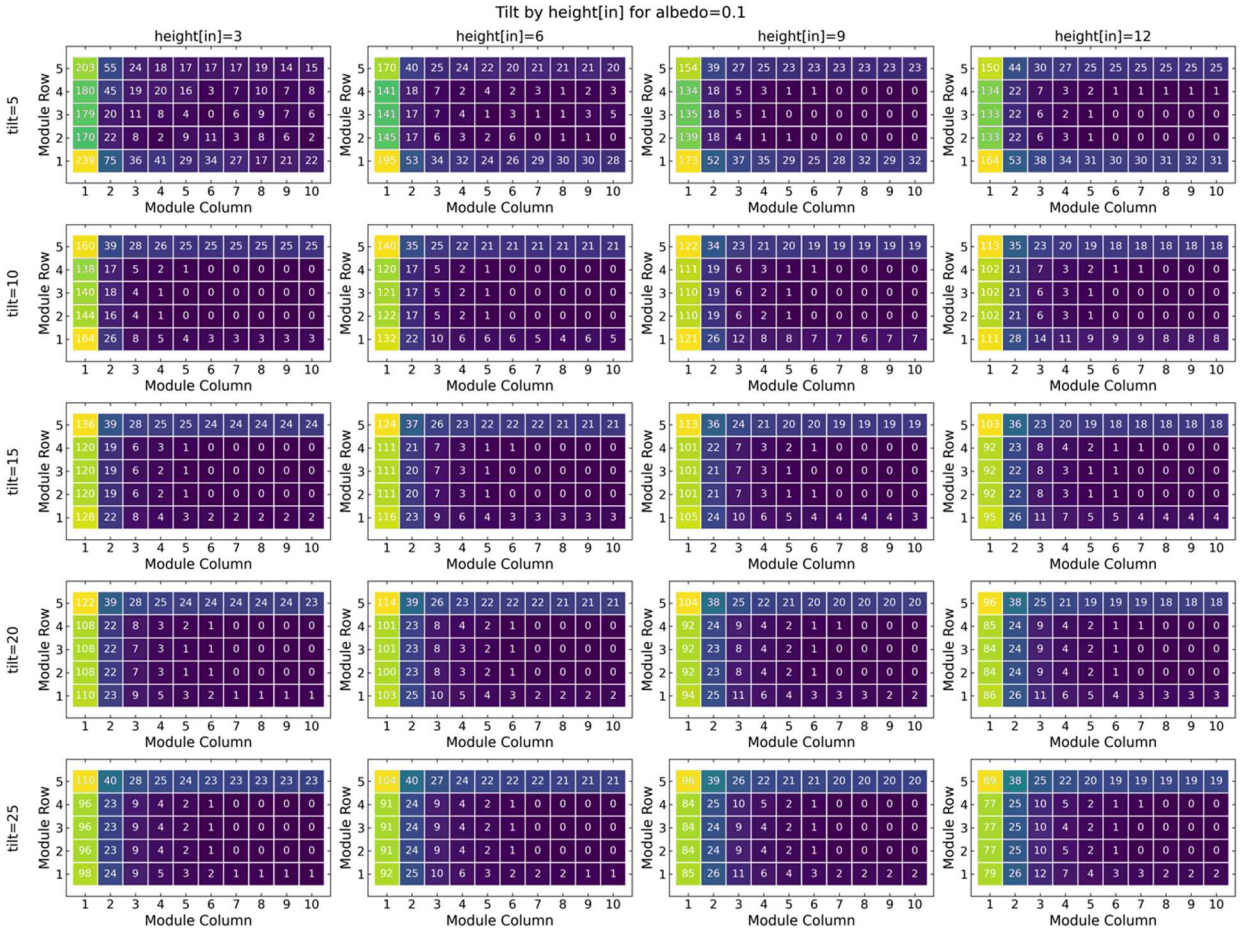


*Figure 19: Matrix view of the western half of five-row systems showing percent increase in rear-side irradiation as compared with the center-most module. Each run is at a different tilt angle and pitch (row in the matrix) and module height (column in the matrix).*

From this singular visualization, the radial increase in rear irradiance from the center module (row 3, column 10) can be observed. The row-to-row difference observed is most notable in the array corners. As array tilt increases, the northern-most (back) row receives more rear irradiance compared with the lower tilt angle case, which shows increased rear-side irradiance on the front row.

These matrix simulations demonstrate a saturation of backside irradiance for modules located away from the edges of the system. This saturation occurs within seven to nine modules from the east and west edges and within three to four rows from the north and south edges. Therefore, simulating more rows or more modules per row does not add any new information.

To take advantage of this saturation, we developed a technique to use these half-system simulations as templates to build larger systems. Figure 20 shows how small-template systems can represent larger systems. The corners and sides of the template systems surround the larger systems while center modules are simply repeated in the areas that are far enough from the edges to experience any edge effects.

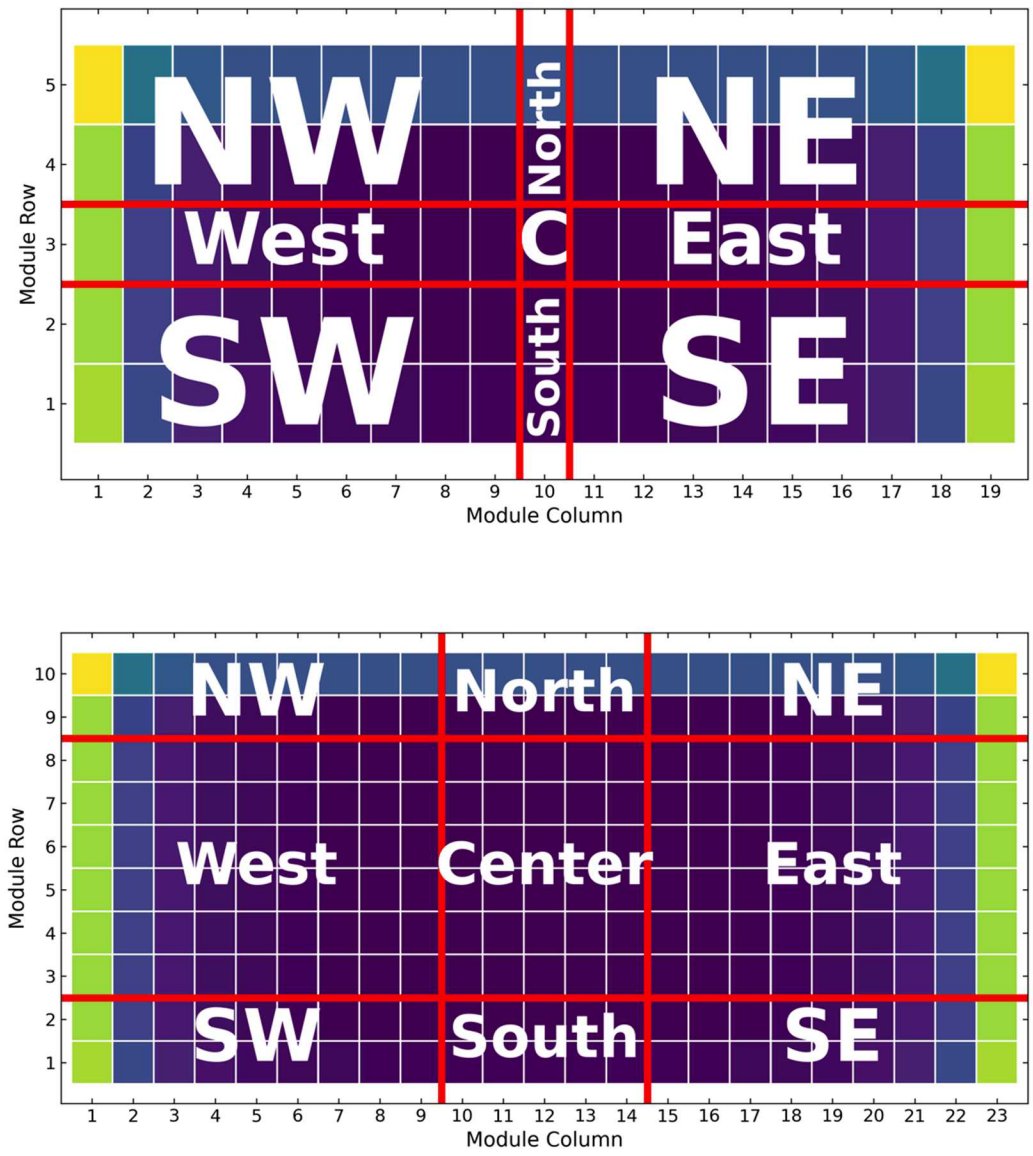


*Figure 20: (top) Classification of the template system regions; (bottom: Application of classified regions to a larger array geometry.*

Figure 20 demonstrates the "stretching" of the cardinal directions (north, south, east, and west) where the section above is replicated to adjacent rows or columns. The corners of the template array (north-west, south-west, south-east, north-east) stay the same size as the template since they are exposed to their unique edge effects.

Next we used this technique on the parametric simulations shown in Figure 19 to investigate the effects of edge effects on a wider variety of system configurations. We first studied the effect of the aspect ratio (number of rows vs. number of modules per row) on system bifacial gains. In this

example, we examined six different system aspect ratios, two albedos, four heights, and five tilt angles. The aspect ratios we considered are listed in Table 1. Results of the impact of these factors, highlighted in Figure 21, show that albedo is of primary importance to bifacial gains, followed by tilt angle and height. The aspect ratio shows a slight increase in bifacial gain for more narrow systems east-to-west. However, this effect is more heavily dominated by system height and tilt angle.

*Table 1. System aspect ratios examined in parameter study of their effect on bifacial gain.*

| Aspect Ratio | Number of rows | Number of modules per row |
|---|---|---|
| 1:25 | 5 | 125 |
| 1:6 | 9 | 69 |
| 1:3 | 15 | 43 |
| 1:2 | 19 | 33 |
| 1:1 | 25 | 25 |
| 2:1 | 33 | 19 |

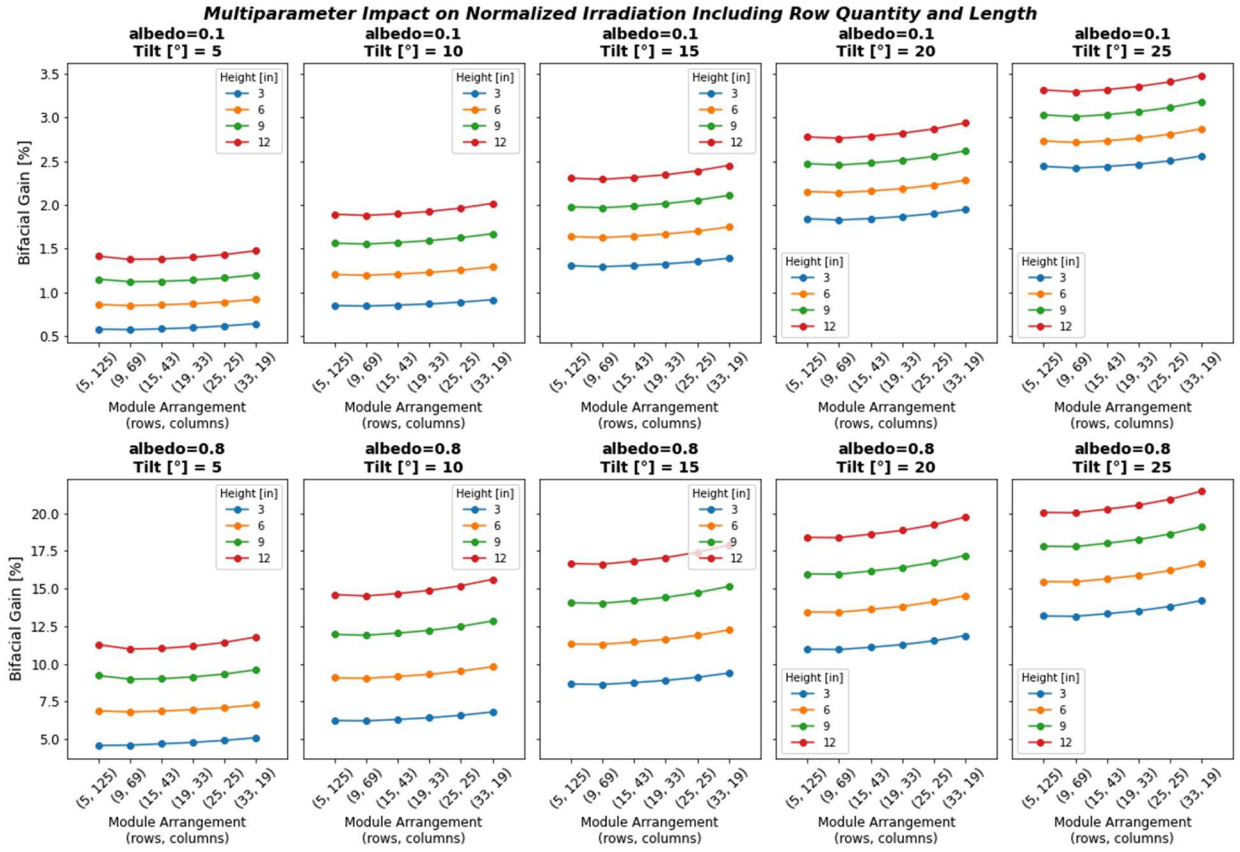


*Figure 21: Annual bifacial gain for fixed-tilt systems with varying albedo (rows), tilt angle (columns) and height (lines) for different aspect ratios (x-axis).*

### Implications for area constrained bifacial systems

The previous example did not consider land usage. The next example focuses on maximizing energy per area and system investment more specifically. For this example, we constrained the system to a 100 m x 100 m square area and allowed the tilt angle–based pitch calculation determine the size of the system. The template systems were then used to describe the overall power generation.

Figure 22 shows the results of the space-constrained fixed-tilt bifacial example. Increasing tilt also increases row spacing (pitch), which lowers the total number of modules in the system and reduces the energy produced. Figure 23 shows the same results in terms of energy produced per module, which has the opposite trend. Each module produces more energy as tilt angle increases, largely due to the same factors the affect monofacial arrays. Higher albedo increases the slope of this effect. The curvature of the increase suggests that there are diminishing returns for increasing module tilt.

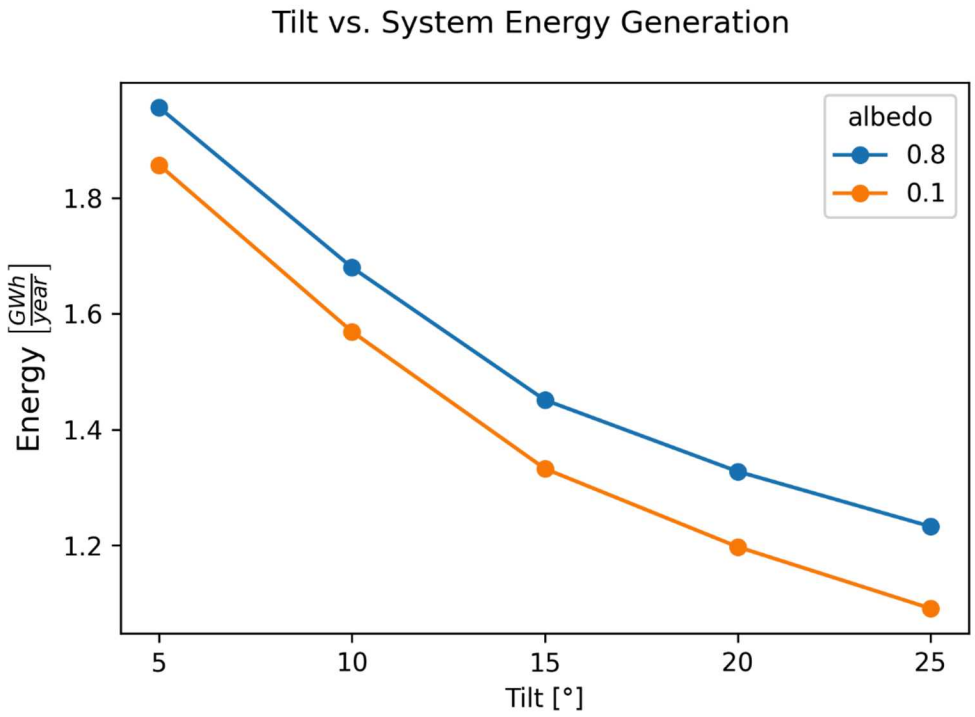


*Figure 22: Bifacial array energy produced as a function of tilt angle for a fixed array area*

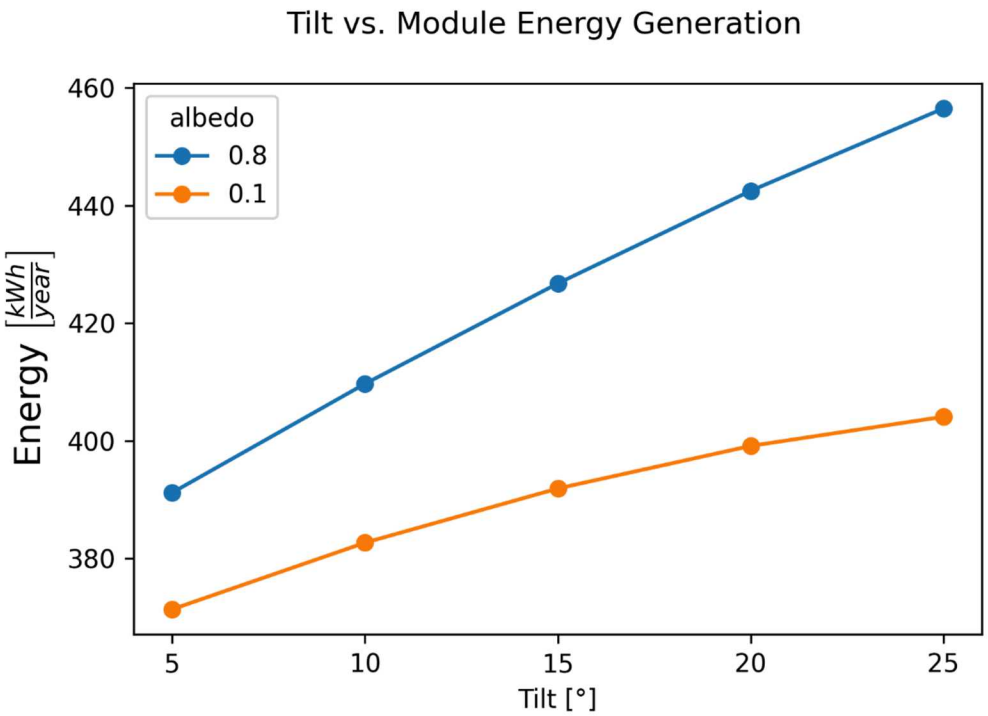


*Figure 23: Bifacial energy produced per module as a function of tilt angle for a fixed array area*

These simulations underscore the importance of considering numerous factors when designing a south-facing fixed-tilt bifacial PV system. In most cases, albedo will likely be the most important factor in determining the degree of bifacial gain, but tilt and height are also key. If racking system costs allow and area is not constrained, raising the system higher off the ground (or roof) and increasing tilt angle may increase bifacial gains. Use of microinverters or DC optimizers to optimize bifacial system edge effects might increase the energy yield of a given design. Clearly, the contributing costs associated with these choices need to be weighed against the potential advantages. Overall, the studies described above provide a sense for the dynamics at play for generalized south-facing fixed tilt-bifacial systems. This information will be used to help design the optimization runs planned for this fall.

### Subtask 3.3: Develop reduced order bifacial performance suitable for desktop computing platforms.

A reduced order model for the electrical mismatch was presented in the previous report and published in Progress in Photovoltaics (Deline et. al, 2020).

The full reduced order bifacial performance model is planned to begin in Y3.

## Task 4. Stakeholder outreach (industry requests, standards development, publications, workshops)

### Subtask 4.1: Distribute publications, software, data, and other relevant information

The following publications and presentations occurred during the current reporting period.

- Ayala Pelaez, S. and C. Deline (2020). "bifacial_radiance: a python package for modeling bifacial solar photovoltaic systems." Journal of Open Source Software 5(50). https://doi.org/10.21105/joss.01865.
- Deline, C., S. A. Pelaez, S. MacAlpine and C. Olalla (2020). "Estimating and parameterizing mismatch power loss in bifacial photovoltaic systems." Progress in Photovoltaics. https://doi.org/10.1002/pip.3259.
- Rodríguez-Gallegos, C. D., H. Liu, O. Gandhi, J. P. Singh, V. Krishnamurthy, A. Kumar, J. S. Stein, S. Wang, L. Li, T. Reindl and I. M. Peters (2020). "Global techno-economic performance of bifacial and tracking PV systems." Joule. https://doi.org/10.1016/j.joule.2020.05.005
- Marion, B., "Albedo Data Sets for Bifacial PV Systems," in 2020 IEEE 47th PVSC, 2020.
- Gostein, M., Marion, B., Stueve, B., "Spectral Effects in Albedo and Rearside Irradiance Measurement for Bifacial Performance Estimation," in 2020 IEEE 47th PVSC, 2020.
- Ayala Pelaez, S., Deline, C., Marion, B., Sekulic, B., McDanold, B., Parker J., Stein, J.S. "Field-Array Benchmark of Commercial Bifaical PV Technologies with Publicly Available Data" 47th IEEE PVSC Conference, virtual June 2019.


### Subtask 4.2: Participate in international BiFi working group

Both the BifiPV Hangzhou and BifiPV San Francisco workshops had to be canceled due to the COVID-19 pandemic. In order to not to lose the momentum we have started with the BifiPV series, we decided to organize a two-day virtual BifiPV Workshop on July 27 & 28, 2020. We have planned four sessions:

July 27 (8:00 TO 11:30 PDT):
- Session 1: BifiPV Technology Updates
- Session 2: Field Results and Validation

July 28 (14:00 TO 16:30 PDT):
- Session 3: Real-World Insights
- Session 4: Reliability & Standards

We have currently 13 speakers lined up with talks in these four areas, from more than 8 countries. There are also more than 750 registrants from 53 countries.


*Figure 24 - Invited speakers and sessions at the virtual bifiPV Workshop on July 27th-28th 2020*

## Subtask 4.3: Participate in industry standards groups on bifacial related standards

### *Interlaboratory Measurement Round Robin*

An interlaboratory comparison of IEC TS 60904-1-2 was completed comparing the results of a round robin between 21 laboratories (15 of them ISO 17025 accredited laboratories) for bifacial module measurement. Results indicate that measurement accuracy for bifacial modules is comparable to standard monofacial measurement. Accuracy for NREL measurements was within 0.5 standard deviations of all Tier-1 labs, indicating good consistency and absolute match with other international las.

Inspired by this international effort, NREL, Sandia, CFV, PVEL and RETC conducted a follow-up round-robin, with 2 bifacial and 1 monofacial modules. Final results show absolute measurement of power among the four labs (Pmax – Pmin) / avg = 3.5% for the monofacial test sample, 3.0% for bifacial sample front-side measurement, and 4.8% for bifacial sample rear-side measurement. The measurement of module bifaciality (P_rear / P_front) was more accurate, coming within 1.3% of each other due to cancelling of bias errors.

### *Bifacial system maximum currents:*

Because bifacial photovoltaic arrays generate current from light received from the back as well as the front of the array, DC currents from bifacial systems are generally higher than for monofacial arrays, which receive light from only the front side of the array. To ensure that these higher currents do not overload bifacial system components (e.g., fuses, wires, etc.) and cause safety issues the factors that influence the DC current of bifacial PV modules should be considered during system design and component selection. Such factors include module performance parameters, ground albedo, and system design parameters (e.g., size, tilt, azimuth, height, number of rows, and row spacing).

Sandia National Laboratories analyzed more than four years of DC current measurements from bifacial and monofacial PV single-module systems in three different U.S. climates to determine the frequency and magnitude of the high current events and correlate these values to system design parameters.

To obtain measurements, Sandia installed bifacial and monofacial modules in three locations with different climates: New Mexico, Vermont, and Nevada. Each location has 32 modules (16 bifacial and 16 monofacial) installed over a range of albedo values, tilt angles, and azimuths. In many cases, the incident irradiance causes the modules to produce power in excess of the maximum input power of their attached microinverter, resulting in inverter clipping. Of particular interest in this study is the DC maximum power current ($I_{MP}$) produced by each module and the irradiance conditions at each site. This work has been accepted for an oral presentation at the EU PVSEC virtual conference in September 2020.

Table 2 describes the orientations and conditions at each site and summarizes the data used in the analysis. Systems 1 through 3 at each site have four monofacial and four bifacial PV modules, and systems 4 and 5 contain two monofacial and two bifacial modules. Each module is grid-connected by a microinverter and monitored for DC current and voltage. The irradiance falling on the front and rear side of all PV systems is measured by a pair of reference cells mounted near the center of each system. All monitored values are 1-min averages of measurements made every five seconds.

For each module at each site, analysts plotted measured IMP against total irradiance which is the front-side irradiance for monofacial modules and the sum of front-side and rear-side irradiance for bifacial modules. They then created a linear regression of the data, excluding current values below 0.05 A to avoid nighttime data and data from shutdown periods, as well as current values above 10.2 A (inverter self-limiting). The first term of the linear regression (slope) provides an approximate relationship between total irradiance and $I_{MP}$, and analysis shows the value of the regression fit evaluated at the maximum total irradiance in the observation period, which is an estimate of the maximum current in the absence of inverter clipping (Figure 25).

They also analyzed empirical cumulative distribution functions for the front, rear, and total irradiance of each orientation. Analysis of the top 1% of irradiances provides a sense of the high irradiances at each site and orientation. The cumulative distribution function for total irradiance can be combined with the regression equation to estimate the probability of exceeding a given current over the observation period with a bifacial PV module. Table 3 summarizes results of 1-minute maximum currents and total irradiances for the bifacial modules, which are important for fuse sizing. Table 4 shows the same quantities for 3-hour averages, which are important for evaluating wire sizing requirements for bifacial arrays.

These results demonstrate that bifacial PV systems operate at significantly higher DC currents than do similar monofacial systems. The highest currents occur as the result of high albedo (e.g. snowfall) and brief but very high irradiance periods likely caused by sunny conditions with cloud enhancement. These results are being shared with industry to support updates to the National Electrical Code for integrating bifacial PV. The results will also help PV designers optimize the

designs of bifacial PV systems to minimize systems costs while creating systems able to safely handle the extra electrical current that is produced from bifacial modules. This work has been accepted for an oral presentation at the EU PVSEC virtual conference in September 2020.

*Table 2: Summary of site and experimental data*

| Site | Albuquerque, New Mexico | Henderson, Nevada | Burlington, Vermont |
|---|---|---|---|
| Data Start Date | 2016-02-16 00:00 | 2016-12-24 00:00 | 2017-03-29 00:00 |
| Data End Date | 2020-07-01 09:29 | 2020-07-01 11:30 | 2019-04-01 08:41 |
| Number of observations | 2,218,361 | 1,850,648 | 869,540 |
| Natural Albedo | 0.22 | 0.2 | 0.18-0.22 (depends on grass condition) |
| Enhanced Albedo | 0.6 | 0.3 | 0.25 |
| System Orientation 1 | West-facing, 15° tilt, high albedo | West-facing, 15° tilt, high albedo | West-facing, 30° tilt, high albedo |
| System Orientation 2 | South-facing, 15° tilt, high albedo | South-facing, 15° tilt, high albedo | South-facing, 30° tilt, high albedo |
| System Orientation 3 | South-facing, 30° tilt, natural albedo | South-facing, 30° tilt, natural albedo | South-facing, 30° tilt, natural albedo |
| System Orientation 4 | South-facing, 90° tilt | South-facing, 90° tilt | South-facing, 90° tilt |
| System Orientation 5 | West-facing, 90° tilt | West-facing, 90° tilt | West-facing, 90° tilt |

*Table 3: One-minute total irradiance measured on bifacial modules at each site and expected maximum current without inverter self-limiting*

| | Albuquerque, New Mexico | | Henderson, Nevada | | Burlington, Vermont | |
|---|---|---|---|---|---|---|
| System | Max Current | Max Irradiance | Max Current | Max Irradiance | Max Current | Max Irradiance |
| 1 | 15.3-15.9A | 2167 W/m$^2$ | 13.6-13.7A | 1672 W/m$^2$ | 12.5-13.1A | 1593 W/m$^2$ |
| 2 | 15.1-15.7A | 2050 W/m$^2$ | 13.8-14A | 1708 W/m$^2$ | 14.9-15.6A | 1885 W/m$^2$ |
| 3 | 13.3-13.4A | 1646 W/m$^2$ | 13.4-13.7A | 1668 W/m$^2$ | 14-14.7A | 1765 W/m$^2$ |
| 4 | 10.9-11A | 1310 W/m$^2$ | 11-11.1A | 1302 W/m$^2$ | 14.5A | 1885 W/m$^2$ |
| 5 | 9.6-9.8A | 1273 W/m$^2$ | 9.4A | 1207 W/m$^2$ | 11-11.1A | 1468 W/m$^2$ |

*Table 4: Three-hour average total irradiance measured on bifacial modules at each site and expected maximum current without inverter self-limiting*

| | Albuquerque, New Mexico | | Henderson, Nevada | | Burlington, Vermont | |
|---|---|---|---|---|---|---|
| System | Max Current | Max Irradiance | Max Current | Max Irradiance | Max Current | Max Irradiance |
| 1 | 10.4-11.2A | 1520 W/m$^2$ | 9.9-10A | 1225 W/m$^2$ | 8.8-9.2A | 1120 W/m$^2$ |
| 2 | 11.5-11.9A | 1566 W/m$^2$ | 10.1-10.3A | 1254 W/m$^2$ | 11.3-11.8A | 1417 W/m$^2$ |
| 3 | 10.3-10.4A | 1276 W/m$^2$ | 10-10.1A | 1238 W/m$^2$ | 11.3-11.8A | 1415 W/m$^2$ |
| 4 | 9.4-9.5A | 1138 W/m$^2$ | 8.5-8.6A | 1012 W/m$^2$ | 10.5A | 1353 W/m$^2$ |
| 5 | 7.7A | 1009 W/m$^2$ | 7.6A | 979 W/m$^2$ | 8.7A | 1153 W/m$^2$ |

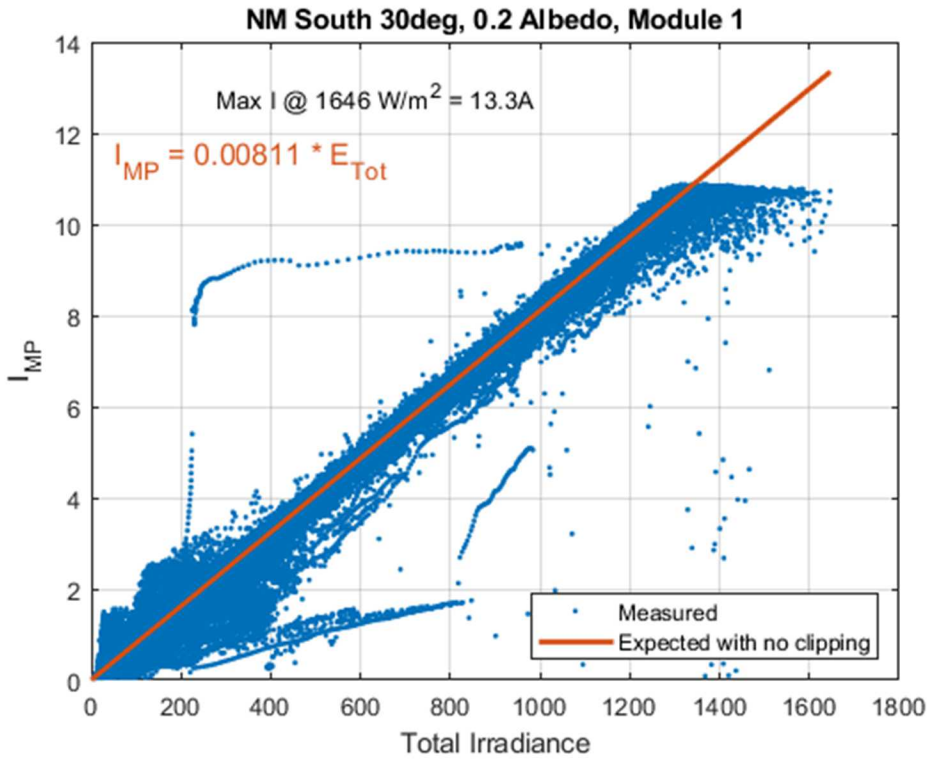


*Figure 25: Example scatter plot of 1-min Imp values from a bifacial module in New Mexico plotted against total irradiance (front + rear). Red regression line extends to the maximum measured total irradiance. Maximum 1-min current is estimated from the Imp value at the maximum total irradiance.*

## Task 6. Albedo Assessments for Bifacial PV Systems

For addition to the albedo data sets that can be accessed from the DuraMat website, three organizations have contributed data for six more locations:

- Canadian Solar, Inc. - desert location near Wuhai, Inner Mongolia, China.
- Technical University of Denmark - grass surface in Roskilde, Denmark.

- 7X Energy – planned PV installation sites near Fayette, Ohio; Pearsall, Texas; Sabinal, Texas; and Coyanosa, Texas.

The NSRDB albedos based on satellite derived MODIS albedo products were compared with SURFRAD network measurements of albedo for 1998 through 2018. The results of this comparison are shown in Table 5. The mean bias difference (MBD) for the annual albedo was from -21 to +28% and the root-mean-square difference (RMSD) was from 7.7 to 29.4%. Considering the 95% confidence interval to be twice the RMSD, the uncertainty of the NSRDB annual albedo is from 15 to 59%, depending on location. Clearly, for some locations, the uncertainty of the NSRDB albedo is too large.

*Table 5: Yearly NSRDB Albedo Versus SURFRAD Albedo*

| Station | Albedo Mean | MBD (%) | RMSD (%) |
|---|---|---|---|
| Bondville IL | 0.248 | -13.9 | 14.7 |
| Boulder CO | 0.197 | 27.5 | 29.4 |
| Desert Rock NV | 0.211 | -10.3 | 10.6 |
| Fort Peck MT | 0.244 | 4.9 | 13.0 |
| Goodwin Creek MS | 0.200 | -20.9 | 21.3 |
| Penn State PA | 0.252 | -5.3 | 7.7 |
| Sioux Falls SD | 0.238 | 12.5 | 16.2 |

The 4km NSRDB grid cell viewed by the satellite encompasses an area much greater than viewed by the SURFRAD albedometer, or a bifacial PV installation for that matter. Consequently, unless the ground surface is uniform within the 4 km grid cell, the NSRDB albedo may not represent what the albedometer or PV system experiences. An example is shown in Figure 26 for the Goodwin Creek station. The SURFRAD station location is in an area that appears brighter than most of the grid cell, a plausible explanation for why the NSRDB data underestimates the albedo measurements.

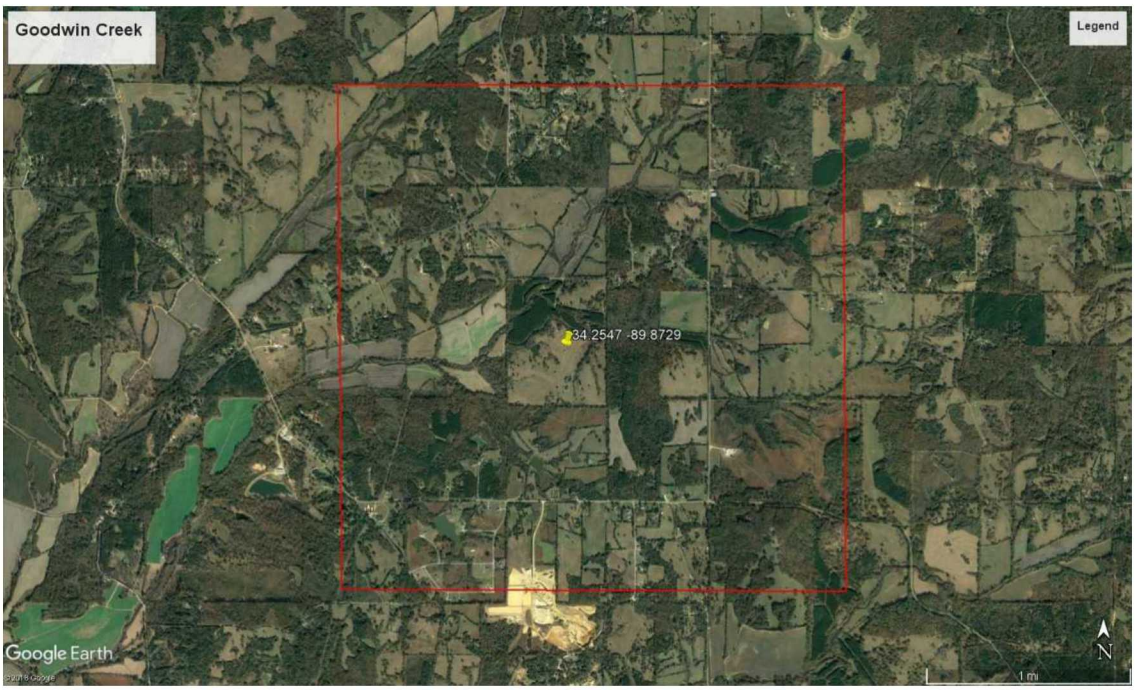

*Figure 26: Google Earth image of Goodwin Creek station location. NSRDB 4 km cell outlined in red, station located at yellow pin. Cell is generally darker than station location, resulting in underestimating albedo at station location.*

## Participants and Collaborators:

- Joshua S. Stein PhD., Principle Investigator, Sandia National Laboratories
- Chris Deline, PhD., Co-PI, National Renewable Energy Laboratory
- Silvana Ayala Pelaez, PostDoc, National Renewable Energy Laboratory
    - Ray tracing modeling, bifacial_radiance developer
- Cameron Stark, Technologist, Sandia National Laboratories
    - High performance computing integration
    - Sensitivity studies and optimization
    - *Cameron left our group for another job at Sandia in June 2020.*
- Bill Marion, Principal Engineer, National Renewable Energy Laboratory
    - Albedo database
- Mark Monarch, Summer Student Intern, National Renewable Energy Laboratory
    - Bifacial_radiance spectral simulations and high-performance computing integration.
- Charles Robinson, Technologist, Sandia National Laboratories
    - Module characterization and testing
- Joseph Coston, Student Intern (NMT), Sandia National Laboratories
    - Building miniaturized bifacial single axis tracker testbed
- Ben Pierce, Student Intern (CWRU), Sandia National Laboratories
    - Machine learning SAT control algorithm development for bifacial

## Plans for Next Reporting Period:

- Bifacial dual-use system results and simulations.
- Bifacial_radiance release and training for users with Amazon Web Services (AWS).
- Optimization study of bifacial PV using DAKOTA
- Prepare for and attend 2020 BifiPV virtual Workshop

## Changes/Problems:

We have not identified any specific problems in the project or suggest any specific changes at this time.